Atmos. Chem. Phys., 21, 11405–11421, 2021
https://doi.org/10.5194/acp-21-11405-2021

Atmospheric Chemistry and Physics
Open Access
EGU

Reduced light absorption of black carbon (BC) and its influence on BC-boundary-layer interactions during "APEC Blue"

Meng Gao[1,2,9], Yang Yang[1], Hong Liao[1], Bin Zhu[3], Yuxuan Zhang[4], Zirui Liu[5], Xiao Lu[6], Chen Wang[7], Qiming Zhou[2], Yuesi Wang[5], Qiang Zhang[8], Gregory R. Carmichael[7], and Jianlin Hu[1]

[1]Collaborative Innovation Center of Atmospheric Environment and Equipment Technology, Jiangsu Key Laboratory of Atmospheric Environment Monitoring and Pollution Control (AEMPC), Nanjing University of Information Science & Technology, Nanjing, 210044, China
[2]Department of Geography, State Key Laboratory of Environmental and Biological Analysis, Hong Kong Baptist University, Hong Kong SAR, 999077, China
[3]Key Laboratory for Aerosol-Cloud-Precipitation of China Meteorological Administration, Nanjing University of Information Science & Technology, Nanjing, 210044, China
[4]School of Atmospheric Sciences, Nanjing University, Nanjing, 210023, China
[5]State Key Laboratory of Atmospheric Boundary Layer Physics and Atmospheric Chemistry, Institute of Atmospheric Physics, Chinese Academy of Sciences, Beijing, 100029, China
[6]School of Atmospheric Sciences, Sun Yat-Sen University, Zhuhai 519082, China
[7]Department of Chemical and Biochemical Engineering, The University of Iowa, Iowa City, IA 52242, USA
[8]Ministry of Education Key Laboratory for Earth System Modeling, Department of Earth System Science, Tsinghua University, Beijing, 100084, China
[9]Hong Kong Branch of Southern Marine Science and Engineering Guangdong Laboratory (Guangzhou), Hong Kong SAR, 999077, China

Correspondence: Meng Gao (mmgao2@hkbu.edu.hk) and Jianlin Hu (jianlinhu@nuist.edu.cn)

Received: 25 February 2021 – Discussion started: 17 March 2021
Revised: 22 June 2021 – Accepted: 24 June 2021 – Published: 29 July 2021

Abstract. Light absorption and radiative forcing of black carbon (BC) is influenced by both BC itself and its interactions with other aerosol chemical compositions. Although the changes in BC concentrations in response to emission reduction measures have been well documented, the influence of emission reductions on the light absorption properties of BC and its influence on BC-boundary-layer interactions has been less explored. In this study, we used the online coupled WRF-Chem model to examine how emission control measures during the Asia-Pacific Economic Cooperation (APEC) summit affect the mixing state and light absorption of BC, and the associated implications for BC-PBL interactions. We found that both the mass concentration of BC and the BC coating materials declined during the APEC week, which reduced the light absorption and light absorption enhancement (E_{ab}) of BC. The reduced absorption aerosol optical depth (AAOD) during APEC was caused by both the decline in the mass concentration of BC itself (52.0 %), and the lensing effect of BC (48.0 %). The reduction in coating materials (39.4 %) contributed the most to the influence of the lensing effect, and the reduced light absorption capability (E_{ab}) contributed 3.2 % to the total reduction in AAOD. Reduced light absorption of BC due to emission control during APEC enhanced planetary boundary layer height (PBLH) by 8.2 m. $PM_{2.5}$ and O_3 were found to have different responses to the changes in the light absorption of BC. Reduced light absorption of BC due to emission reductions decreased near-surface $PM_{2.5}$ concentrations but near-surface O_3 concentrations were enhanced in the North China Plain. These results suggest that current measures to control SO_2, NO_x, etc. would be effective in reducing the absorption enhancement of BC and in inhibiting the feedback of BC on the boundary layer. However, enhanced ground O_3 might be a side effect of current emission control strategies. How to control emissions

to offset this side effect of current emission control measures on O_3 should be an area of further focus.

1 Introduction

Black carbon (BC) in the atmosphere is produced both naturally and by human activities, attributable to the incomplete combustion of hydrocarbons (Bond et al., 2013; Ramanathan and Carmichael, 2008). In addition to contributing to particulate matter and degraded air quality, it is the dominant absorber of visible solar radiation, playing a unique and pivotal role in the Earth's climate system (Bond et al., 2013; Menon et al., 2002; Ramanathan and Carmichael, 2008; Yang et al., 2019). The absorption of BC occurs not only in the atmosphere, but also when it is deposited over snow or ice, and it triggers positive feedback and exerts positive radiative forcing (Flanner et la., 2007; Grieshop et al., 2009). The direct radiative forcing of atmospheric black carbon was estimated to be $0.4\,W\,m^{-2}$ ($0.05–0.8\,W\,m^{-2}$) (IPCC, 2014), and BC has been targeted in emission control policies to mitigate both air pollution and global warming (Grieshop et al., 2009).

Before the 1950s, intense emissions of BC were concentrated in North America and Western Europe. In recent decades, South and East Asia have emerged to become major source regions (Ramanathan and Carmichael, 2008). BC emitted from China is responsible for a quarter of total global emissions (Bond et al., 2004). Chemical transport model simulations suggest that the residential sector is the leading source for mass concentration of BC in China, followed by the industrial sector (Li et al., 2016). Mean BC direct radiative forcing in China is $\sim 1.22\,W\,m^{-2}$, more than three times the global mean forcing (Li et al., 2016), two-thirds to three-fourths of which were contributed by local emissions of BC in China, and the rest by emissions in other countries (Li et al., 2016; Yang et al., 2017).

Specific policies to address BC emissions have not been implemented in China, yet multiple measures targeting $PM_{2.5}$ reduction have resulted in declines in BC (Gao et al., 2018b; Yamineva and Liu, 2019). A number of observational studies have revealed the declining trend of BC concentrations in China in recent years (Ji et al., 2018, 2019a, b; Qin et al., 2019). From 2013 to 2018, the annual mean BC concentrations in Beijing declined from 4.0 to $2.6\,\mu g\,m^{-3}$ (Ji et al., 2019b). Associated changes in BC radiative forcing can be expected from declines in mass concentration of BC in China, while the radiative forcing of BC is influenced also by the changes in other aerosol components.

BC absorption is closely connected with the aging process, which is defined as the interaction between BC and other aerosol chemical compositions (Jacobson, 2001). After being emitted from combustion processes, BC particles can coagulate and grow by condensation, during which both self-coagulation and heterocoagulation happen (Jacobson, 2001). Although BC is mixed internally with other components, it is impossible for the system to be well-mixed, due to the irregular shape of BC (Jacobson, 2001). A core-shell morphology is commonly established, with BC as the core and the coating materials (organics, sulfate, etc.) as the shell (Jacobson, 2001; Zhang et al., 2018). Numerous efforts have been made to explore the influence of aerosol components on internally mixed BC absorption (Cappa et al., 2012; Chen et al., 2021; Bond et al., 2006; Fuller et al., 1999; Jacobson, 2001; D. Liu et al., 2017; Onasch et al., 2012; Peng et al., 2016). It was proposed that the coating components (shell) could act as a lens to focus more photons onto the core to enhance the light absorption of BC (Fuller et al., 1999). Bond et al. (2006) estimated that this lensing effect would increase the light absorption of BC by 50 %–100 %. Jacobson (2001) reported a global average BC absorption enhancement factor of 2, whereas other values, from negligible (Cappa et al., 2012) to as high as 2.4 (Peng et al., 2016) have also been previously found. This lensing effect has also been recognized as an important factor affecting the radiative forcing of BC (Jacobson, 2001). In the last decade, efforts were also made to develop models to predict the dynamic evolution of aerosol mixing states (Ching et al., 2016; Curtis et al., 2017; Matsui et al., 2013; Tian et al., 2014). For example, Matsui et al. (2013) developed a 2D aerosol bin scheme that can resolve BC mixing state and BC aging processes. However, these approaches are far too computationally expensive for use in regional 3D models (Barnard et al., 2010).

Over the past several years, the State Council of China has issued a comprehensive Air Pollution Prevention and Control Action Plan (APPCAP), covering major emission sectors (Liang et al., 2017; Q. Zhang et al., 2019). Long-term observations of aerosol chemical composition indicate that both concentrations of BC and other coating components have declined rapidly (Gao et al., 2020b; Ji et al., 2019b; Zhou et al., 2019). Although the changes in BC concentrations in response to emission reduction measures have been documented (Ji et al., 2019b; Gao et al., 2020b), the influence of emission reductions on the aging processes and light absorption of BC has been less explored (Y. Zhang et al., 2019b). Zhang et al. (2018) observed that the declines in absorption of BC was mainly due to decreases in BC mass concentration (86 %), and that the weakening of BC light absorption capability also played a role (14 %). However, this finding was formulated based on surface observations; little is known about the changes at upper layers. Given the importance of BC absorption in the upper boundary layer to the buildup of pollution (Ding et al., 2016), the impact of emission reductions on the light absorption of BC, and its implications for the development of boundary layer and pollution episodes, it needs further investigation. On 5–11 November 2014, Beijing, China hosted the Asia-Pacific Economic Cooperation (APEC) conference, during which Beijing and surrounding regions cooperated to implement short-term emission control measures to ensure good air quality. This event offers a

great opportunity to study atmospheric composition and its physical and chemical responses to emission reductions.

In this study, we address the following questions using the APEC event as a case study: (1) how did emission reductions affect the aging processes and light absorption of BC during APEC; (2) what were the relative contributions of reduced mass concentrations of BC, aging processes of BC, and the reshaped mixing state of BC to the changes in light absorption of BC during APEC; and (3) how did these processes affect BC-PBL interactions and the formation of air pollution? In Sect. 2, we describe the WRF-Chem model configurations and the observational data sets used in this study. Results are presented in Sect. 3, and conclusions and discussions are provided in Sect. 4.

2 Methods and data

2.1 WRF-Chem model configuration

Version 3.8.1 of the WRF-Chem model (Grell et al., 2005) was adopted in this study to simulate the emission, chemical transformation, and deposition of aerosols, as well as their interactions with radiation. We demonstrated in previous studies (Gao et al., 2016a, b, 2020b, c) that the spatiotemporal variations of air pollutants over China could be reproduced effectively by WRF-Chem. WRF-Chem enables multiple options for gas phase chemistry and aerosol modules (Grell et al., 2005). We employed the carbon bond mechanism version Z (CBMZ) gas phase chemistry (Zaveri and Peters, 1999) coupled with the model for simulating aerosol interactions and chemistry (MOSAIC) (Zaveri et al., 2008) aerosol module in this study. MOSAIC treats size-resolved aerosol species, and we used 8 bins version in this study, corresponding to the particle diameter ranges of 0.039–0.078, 0.078–0.156, 0.156–0.312, 0.312–0.625, 0.625–1.25, 1.25–2.5, 2.5–5.0, 5.0–10.0 µm, respectively. Secondary organic aerosol (SOA) formation in MOSAIC was simulated with a volatility basis set (VBS) (Shrivastava et al., 2011). We configured two nested domains with horizontal resolutions of 81 and 27 km, and 31 vertical layers up to a pressure level of 50 hPa. The configured domains cover most areas of East Asia and focus on the North China region (same as Fig. 1 in Gao et al., 2017). Other chosen options for key physical parameterizations follow Gao et al. (2016b). Meteorological initial and boundary conditions were provided by the NCEP $1^\circ \times 1^\circ$ degree final reanalysis data set (FNL), and chemical initial and boundary conditions were obtained from the MOZART global chemistry simulations (Emmons et al., 2010). We used the YSU scheme in WRF-Chem to simulate the evolution of boundary layer, and the YSU scheme defines the top of the boundary layer using the Richardson number (Hong et al., 2010). To allow the effects of aerosol on meteorological conditions in the model, we did not apply observational nudging or reanalysis nudging.

Anthropogenic emissions of particles and gases in China in the model were taken from the multiresolution emission inventory for China (MEIC) for year 2014 developed by Tsinghua University (Zheng et al., 2018). Anthropogenic emissions for areas outside China were obtained from the MIX Asian emission inventory developed for MICS-Asia and HTAP, which combines five emission inventories for Asia (Li et al., 2017). Both MEIC and MIX data sets provide monthly emissions of air pollutants at $0.25^\circ \times 0.25^\circ$ grids, which were interpolated to WRF-Chem modeling domains in this study. We adopted the MEGAN model version 2.04 to estimate biogenic emissions of gases and particles online (Guenther et al., 2006). The global fire emissions database version 4 (GFEDv4) (Giglio et al., 2013) was used for open fire emissions.

We simulated the period from 16 October to 13 November and discarded the first seven days as spin-up to avoid the influence of initial conditions. To explore the influences of coordinated emission control measures on BC absorption, we conducted multiple sets of simulations, as described in Table 1. For the NOCTL experiments, simulations were conducted with no perturbations in emissions. For the CTL experiments, emissions of SO_2, NO_x, PM_{10}, $PM_{2.5}$, VOCs, and other species in Beijing were reduced by 39.2 %, 49.6 %, 66.6 %, 61.6 %, 33.6 %, and 50 %, respectively, over the November 3-11 period. Emissions in Inner Mongolia, Shanxi, Hebei, Tianjin, and Shandong were reduced by 35 %. These perturbation factors were taken from the BMEPB reports (Gao et al., 2017). The locations of these provinces are marked in Fig. 1 in Gao et al. (2017).

The influence of BC absorption under different assumptions, including external and core-shell mixing and with or without emission reductions ($\Delta_{\text{BC-Ext-NOCTL}}$, $\Delta_{\text{BC-Ext-CTL}}$, $\Delta_{\text{BC-CS-NOCTL}}$, $\Delta_{\text{BC-CS-CTL}}$, and $\Delta_{\text{BC-CYSN-CS}}$), can be derived with Eqs. (1)–(5) below. The description of each simulation is documented in Table 1.

$$\Delta_{\text{BC-Ext-NOCTL}} = \text{NOCTL}_{\text{Ext}} - \text{NOCTL}_{\text{Ext-nobc}} \quad (1)$$

$$\Delta_{\text{BC-Ext-CTL}} = \text{CTL}_{\text{Ext}} - \text{CTL}_{\text{Ext-nobc}} \quad (2)$$

$$\Delta_{\text{BC-CS-NOCTL}} = \text{NOCTL}_{\text{CS}} - \text{NOCTL}_{\text{CS-nobc}} \quad (3)$$

$$\Delta_{\text{BC-CS-CTL}} = \text{CTL}_{\text{CS}} - \text{CTL}_{\text{CS-nobc}} \quad (4)$$

$$\Delta_{\text{BC-CS-CYSN}} = \text{CYSN}_{\text{CS}} - \text{CYSN}_{\text{CS-nobc}} \quad (5)$$

The influence of emission reductions during APEC on changes in the light absorption of BC and associated changes in meteorological and pollution conditions under external and core-shell mixing assumptions ($\Delta_{\text{emission-Ext}}$ and $\Delta_{\text{emission-CS}}$) can be inferred with Eqs. (6)–(7) below. We use Eq. (8) to derive the impact of changed BC aging processes by comparing the differences between core-shell simulation and external mixing simulation. The influences of reduced coating due to emission control measures during APEC are calculated with Eq. (9). We use Eq. (10) to derive the influence of changes in the light absorption enhancement (E_{ab}) of

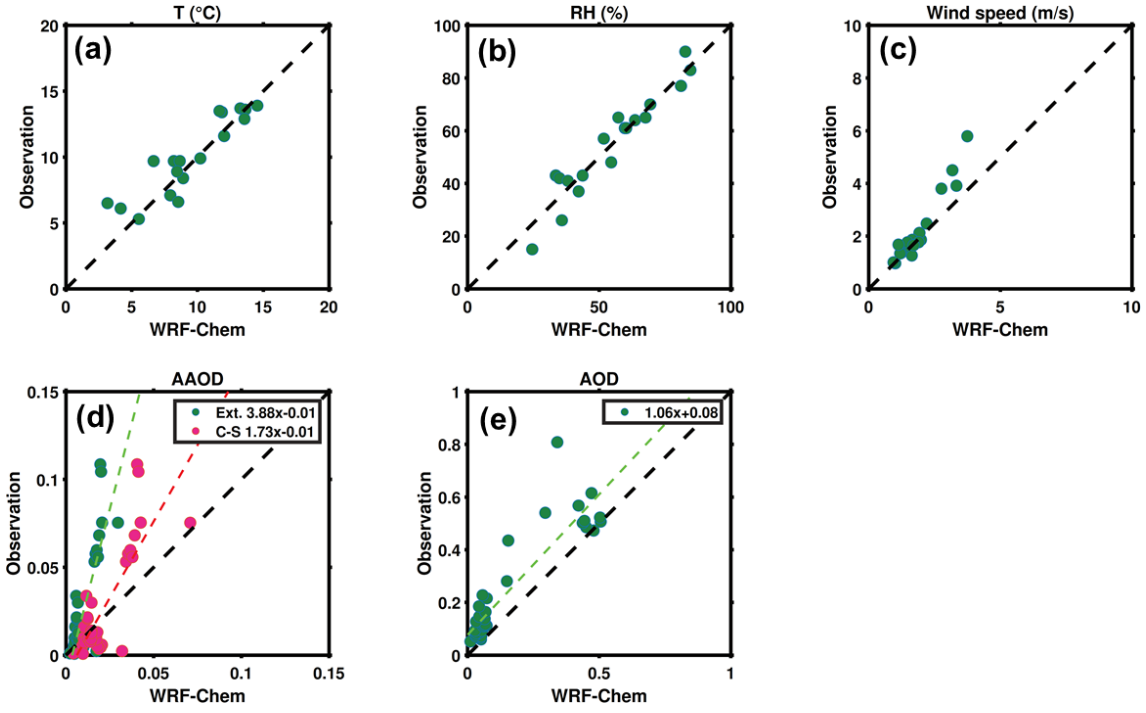

Figure 1. Scatter plots of modeled and observed near-surface meteorological variables (**a**: T, **b**: RH, **c**: wind speed); modeled AAOD with the core-shell model and an external mixing assumption, and the comparisons against observations (**d**); modeled and observed AOD (**e**).

BC.

$$\Delta_{\text{emission-Ext}} = \Delta_{\text{BC-Ext-CTL}} - \Delta_{\text{BC-Ext-NOCTL}} \quad (6)$$

$$\Delta_{\text{emission-CS}} = \Delta_{\text{BC-CS-CTL}} - \Delta_{\text{BC-CS-NOCTL}} \quad (7)$$

$$\Delta_{\text{aging}} = \Delta_{\text{emission-CS}} - \Delta_{\text{emission-Ext}} \quad (8)$$

$$\Delta_{\text{coating}} = \Delta_{\text{BC-CS-CYSN}} - \Delta_{\text{BC-CS-CTL}} \quad (9)$$

$$\Delta_{E_{\text{ab}}} = \frac{\frac{\Delta_{\text{emission-CS}}}{\Delta_{\text{BC-CS-NOCTL}}} - \frac{\Delta_{\text{emission-Ext}}}{\Delta_{\text{BC-Ext-NOCTL}}}}{\frac{\Delta_{\text{emission-CS}}}{\Delta_{\text{BC-CS-NOCTL}}}} \quad (10)$$

2.2 Calculation of aerosol optical properties in WRF-Chem

WRF-Chem uses Mie theory to calculate layer aerosol optical depth (AOD), single scattering albedo (SSA), and asymmetry factor (g). First, the size parameter and spectral refractive index are used to calculate the Mie extinction efficiency Q_{e}. Then, the extinction coefficient $\sigma_{\text{e}}(\lambda)$ is provided by the integral of Q_{e} with consideration of the geometric size of the particle (πr^2) and the particle number size distribution $n(r)$ (Eq. 11). $\sigma_{\text{e}}(\lambda)$ is a equation of wavelength λ. Similarly, absorption coefficient $\sigma_{\text{a}}(\lambda)$ and scattering coefficient $\sigma_{\text{s}}(\lambda)$ can be obtained with Mie absorption efficiency Q_{a} and Mie scattering efficiency Q_{s}. The value of SSA can be calculated with Eq. (12) using $\sigma_{\text{a}}(\lambda)$ and $\sigma_{\text{s}}(\lambda)$.

$$\sigma_{\text{e}}(\lambda) = \int_{r_{\min}}^{r_{\max}} Q_{\text{e}} \pi r^2 n(r) \mathrm{d}r \quad (11)$$

$$\text{SSA}(\lambda) = \frac{\sigma_{\text{s}}(\lambda)}{\sigma_{\text{s}}(\lambda) + \sigma_{\text{a}}(\lambda)} \quad (12)$$

The calculated optical properties vary with the assumption of mixing state of aerosols. For external mixing, each particle is assumed to be a single chemical species. There are several models proposed for internal mixing, and the commonly used ones include the volume averaging model and core-shell model. In the volume averaging model, all species are assumed to be well mixed, while the core-shell model assumes that BC is coated by a well-mixed shell of another species (Jacobson, 2001). The volume-weighted refractive index m is obtained with the equation below:

$$m = \frac{\sum_i V_i m_i}{\sum_i V_i} \quad (13)$$

In Eq. (13), V_i denotes the volume of species i and m_i represents the refractive index of species i. For core-shell internal mixing, similar averaging processes are applied to the core and shell separately. The scattering efficiency, absorption efficiency, and asymmetry parameter are then obtained using the core-shell Mie theory documented in Ackerman and Toon (1981). Core-shell Mie calculations request the core radius, shell radius, refractive index of the core, and refractive

Table 1. Descriptions of model simulations.

Experiments	Descriptions
$NOCTL_{Ext}$	No perturbations in emissions; assuming external mixing of BC.
$NOCTL_{Ext\text{-}nobc}$	No perturbations in emissions; assuming external mixing of BC; assuming no absorption of BC.
$NOCTL_{CS}$	No perturbations in emissions; calculating optical properties using core-shell assumption.
$NOCTL_{CS\text{-}nobc}$	No perturbations in emissions; calculation of optical properties using core-shell assumption; assuming no absorption of BC.
CTL_{Ext}	Emissions are reduced during APEC; assuming external mixing of BC.
$CTL_{Ext\text{-}nobc}$	Emissions are reduced during APEC; assuming external mixing of BC; assuming no absorption of BC.
CTL_{CS}	Emissions are reduced during APEC; calculation of optical properties using core-shell assumption.
$CTL_{CS\text{-}nobc}$	Emissions are reduced during APEC; calculation of optical properties using core-shell assumption; assuming no absorption of BC.
$CYSN_{CS}$	Emissions of BC are reduced while emissions of other species are not during APEC; calculation of optical properties using core-shell assumption.
$CYSN_{CS\text{-}nobc}$	Emissions of BC are reduced while emissions of other species are not during APEC; calculation of optical properties using core-shell assumption; assuming no absorption of BC.

index to the shell as inputs (Ackerman and Toon, 1981; Toon and Ackerman, 1981). The official version of WRF-Chem does not calculate the optical properties of aerosols with an external mixing assumption. To assess the influence of mixing with coating particles on the light absorption of BC, the estimated light absorption of pure BC is required. We modified the optical calculation module in WRF-Chem so that it does not mix BC with other chemical species in the calculation of optical properties. In the calculation of optical properties with an internal mixing assumption, the volume-weighted refractive index are inputs of the Mie code. In the calculation of the optical properties of BC with an external mixing assumption, we only allowed BC to go through the Mie code. The mass and particle number of BC, denoted in M_i and N_i in each bin i (1 through 8) are computed first, and the volume (V_i) is obtained then by dividing by the density of BC. During the calculation of physical diameter (Eq. 14), other chemical species are not considered. Accordingly, BC does not mix with other chemical species, and we designated it as optical properties of BC with an external mixing assumption here. It should be noted that this calculation is different from treatments of external mixing in other models where all particles are separated from each other. In our calculation, BC within each bin are internally mixed, although it does not mix with other chemical species. As the purpose of this study is to explore how coating particles on BC would affect the absorption of BC, this treatment would not be an issue.

$$D_i = 2\left(\frac{\frac{V_i}{N_i}}{\frac{4}{3}\pi}\right)^{\frac{1}{3}} \quad (14)$$

2.3 Observations

Both observations of meteorological variables and air pollutants were used to evaluate the performance of the model over the APEC study period in Gao et al. (2017) and in this study. The meteorological measurements were retrieved from the National Centers for Environmental Information website (https://gis.ncdc.noaa.gov/maps/ncei#app=cdo, last access: 22 July 2021), which includes near-surface temperature, relative humidity (RH), wind speed, and wind direction. The hourly surface concentrations of $PM_{2.5}$ and daily $PM_{2.5}$ chemical compositions were measured at the Institute of Atmospheric Physics (IAP), Chinese Academy of Sciences (CAS) site (Z. Liu et al., 2017; Pan et al., 2012; Yang et al., 2020). We also obtained absorption aerosol optical depth (AAOD) from the AERONET network (Dubovik and King, 2000; Holben et al., 1998) to evaluate model performance. We derived AAOD at 440 nm based on an angstrom exponent relation (Schuster et al., 2006) to make it consistent with observations. Data from more than 500 sites across the world are provided online at the AERONET website (http://aeronet.gsfc.nasa.gov, last access: 22 July 2021).

3 Results

3.1 Model evaluation

Model evaluation was conducted with surface observations of meteorological variables, $PM_{2.5}$, $PM_{2.5}$ chemical components, and AAOD. Data at two meteorological sites in urban Beijing were averaged, and were compared against the model

values for the domain grid cell containing the monitoring site. Figure 1 indicates that the daily mean temperature and relative humidity (RH) are captured well by the model. Observed strong wind conditions are slightly underestimated, which is a common issue due to inaccurate land use inputs or other problems in the model (Gao et al., 2018a). Our previous investigation (Gao et al., 2017) suggested that temperature and RH were lower, and northerly winds became more frequent from before APEC compared with during APEC periods, contributing to pleasant air quality. Figure 2a displays the simulated and observed hourly $PM_{2.5}$ concentrations in urban Beijing. Before APEC, observed high $PM_{2.5}$ concentration is captured well by our model. During APEC, the NOCTL case overestimates $PM_{2.5}$ concentrations, while the CTL case exhibits better agreement with observations. Implementing emission reductions in the model lowers the mean bias of the model from 30.8 to $-4.0\,\mu g\,m^{-3}$. The performance of WRF-Chem in simulating wintertime $PM_{2.5}$ chemical compositions was explored extensively in our previous investigations (Gao et al., 2016b, 2018a). Similarly, measured high concentrations of inorganic aerosols (sulfate, nitrate, and ammonium) are underestimated, which could be partly due to missing sulfate formation pathways (Cheng et al., 2016). We used the updated version with heterogeneous sulfate formation (Gao et al., 2016a) to reduce the underestimation of sulfate in this study. Simulated BC concentration shows a high degree of consistency with observations, while OC is slightly underestimated due to large uncertainties in the current status of SOA modeling (Fig. 2f). In general, the temporal variations and magnitudes of air pollutants are represented effectively in our model. Figure 1d compares simulated AAOD with an external mixing assumption and a core-shell model against AERONET inferred AAOD during the APEC study period. AAOD simulated with an external mixing assumption exhibits much lower values than with observation. With the core-shell model, this underestimation is largely reduced. However, AAOD is still underestimated by the model, which might be caused by missing sources of absorbing particles in the model. Currently, the absorption of organics is not treated in the WRF-Chem model, which is likely to underestimate the light-absorbing capability of carbonaceous aerosols in the atmosphere (Andreae and Gelencsér, 2006). Uncertainties in the aerosol size distribution in emissions may also contribute to this mismatch between the model and observations (Matsui, 2016).

3.2 Reductions in the concentrations of BC and coating pollutants and changes in BC aging degree

Previously, the reductions of air pollutants were estimated by comparing concentrations of air pollutants during the APEC period with those during other periods. Given the differences in meteorological conditions, such a comparison is not able to indicate the influence of emission control measures. As displayed in Fig. 2a, the concentrations during 24–25 October can be two times of those during 26–27 October, although no emission reduction measures were implemented. Previously, we concluded that the meteorological conditions during the APEC week were generally favorable for good air quality compared to it during the week before the APEC week (Gao et al., 2017). Thus, we perturbed emissions in this study to examine how it would affect concentrations of air pollutants, including both BC and its coating pollutants. As displayed in Fig. 3a–b, mean concentrations of SO_2 and NO_2 in urban Beijing declined by 38.7 % and 36.3 %, respectively, in response to short-term emission control measures. Based on observations, Zhang et al. (2018) reported that SO_2 concentrations decreased by 35 % (67 %), and NO_2 concentrations decreased by 34 % (45 %) compared with that before (after) APEC. These declines in aerosol precursors would have modified secondary aerosol formation during the APEC week. Our model indicates that sulfate and nitrate declined by 40.0 % and 28.2 %, respectively. Given the slight underestimation of sulfate and nitrate, these values might have been moderately underestimated. Mass concentrations of BC declined by 34.6 %, while the abundance of OC in the atmosphere exhibited a larger reduction (44.2 %).

We used the ratio of the sum of pollutants (primary as well as secondary) to black carbon concentrations (rBC) to track the relative abundance of BC and non-BC particles, which is essential in the C-S calculation:

$$r\mathrm{BC} = \frac{\begin{array}{c}[\mathrm{sulfate}] + [\mathrm{nitrate}] + [\mathrm{ammonium}] \\ + [\mathrm{organics}] + [\mathrm{dust}] \\ + [\mathrm{sodium}] + [\mathrm{chloride}]\end{array}}{[\mathrm{BC}]}. \quad (15)$$

As shown in Fig. 3c, the impacts of emission reductions during APEC on rBC behave differently at different sizes. For ultrafine particles, emission reductions generally lower the aging degree of BC. This is consistent with the observational evidence that smaller BC cores show larger reductions in aging degree as a result of emission control measures during APEC (Zhang et al., 2018). As most secondary aerosols are in smaller sizes, the effect of emission reduction on BC aging is more significant for smaller particles. Zhang et al. (2018) reported only the changes in sizes below 0.2 µm, our modeling results suggest, however, that the aging degree of BC might be enhanced under emission reductions for relatively larger particles (Fig. 3c). The impact of emission reductions on rBC behaves differently near the surface and at higher layers (Fig. 3d). The aging degree is lowered in the CTL case near the surface, mainly due to reductions in coating materials. However, at layers higher than 200 m, the aging degree of BC increases with emission reductions. In-situ near-surface measurements also indicate that rBC was reduced during APEC, and the reduction was most likely caused by lower photochemical production (Zhang et al., 2018).

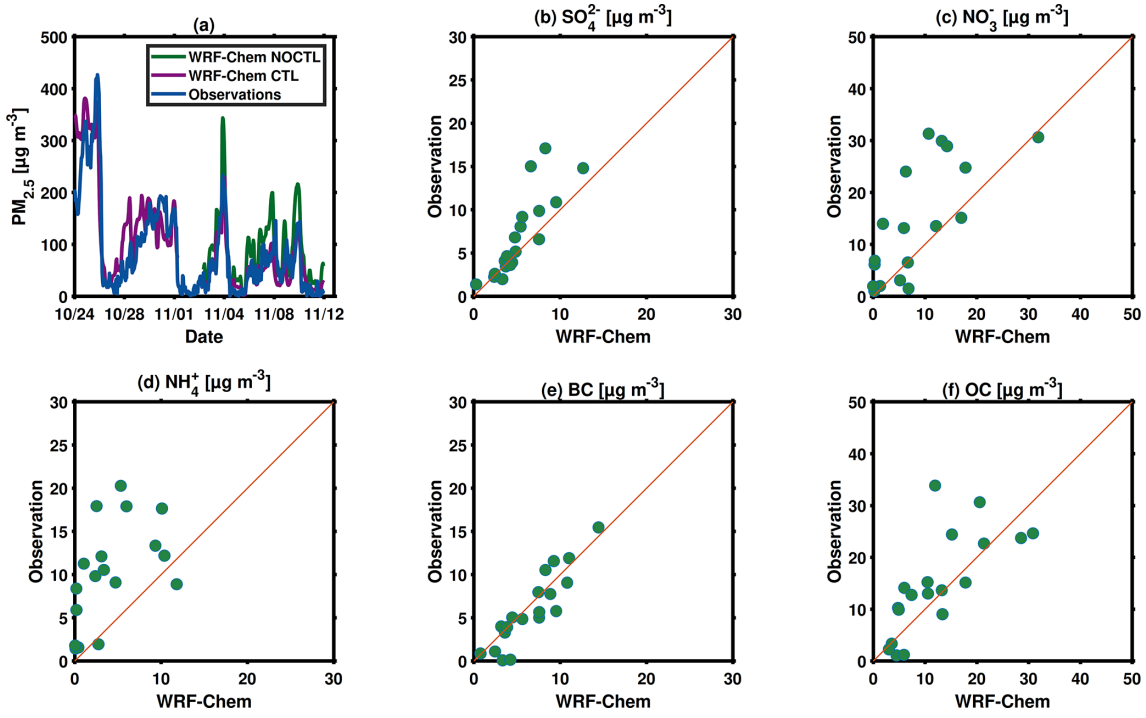

Figure 2. Modeled and observed time series of $PM_{2.5}$ concentrations in urban Beijing **(a)**; Scatter plots of modeled and observed near-surface daily mean concentrations of sulfate, nitrate, ammonium, BC (black carbon), and OC (organics) in Beijing **(b–f)**.

3.3 Changes in AAOD and the light-absorption enhancement (E_{ab}) of BC during APEC

rBC values describe the aging degree of BC, while the exploration of how emission reductions affect light absorption of BC requires a sophisticated calculation of optical properties of BC. Mie theory is commonly used to calculate the light absorption enhancement of BC (E_{ab}) from the lensing effect with a core-shell model. Zhang et al. (2018) estimated E_{ab} by dividing the light-absorption cross section of the whole BC-containing particle by that of the BC core at a certain wavelength. Here we follow the method in Curci et al. (2019), and calculate E_{ab} as the ratio of BC AAOD estimated assuming core-shell internal mixing to that calculated with an external mixing assumption (enhancement due to mixing with coating non-BC particles):

$$E_{ab} = \frac{\text{BC\_AAOD (550 nm, core-shell mixing)}}{\text{BC\_AAOD (550 nm, external mixing)}}$$
$$\text{(AAOD can be either layer or column)}. \quad (16)$$

Inferred vertical profiles of layer E_{ab} values in the CTL and NOCTL scenarios are displayed in Fig. 3e. At the layers below 5 km, mean E_{ab} values are 1.96 and 1.95 for CTL and NOCTL scenarios, respectively. Below 500 m in the troposphere, emission reductions during APEC lower E_{ab} from 2.11 to 2.06. A previous study by Jacobson (2001) suggests a global average BC absorption enhancement factor of 2, which is consistent with the current study. However, a wide range of enhancement factors have been reported, from negligible (Cappa et al., 2012) to as high as 2.4 (Peng et al., 2016). D. Liu et al. (2017) pointed out that the enhancement factors depend on the particles' mass ratio of nonblack carbon to black carbon. Our model results also indicate that the reductions in light absorption enhancement of BC are concentrated at lower layers, while enhancement could happen at higher layers (Fig. 3e). This is consistent with the vertical profile of rBC where it decreases due to emission reductions near the surface, while increasing at higher layers (Fig. 3d).

Figure 4a presents the daytime mean (defined as the mean BC AAOD over the 10:00–17:00 time period) BC AAOD in Beijing inferred from simulations with different mixing assumptions and emission perturbations. In the NOCTL scenarios, BC AAOD simulated with a core-shell model exhibits higher values than those with an external mixing assumption (0.0220 for external and 0.0427 for core-shell). Due to reductions in emissions, these values decline to 0.0145 and 0.0283, respectively. Due to emission reductions (differences between the CTL and NOCTL scenarios), mean daytime BC AAOD decreases by 0.0075 during the APEC week, as a result of declines in mass concentration of BC (52.0 %, Table 2). However, the lensing effect of BC induces a further decline of 0.0069 (48.0 %, Table 2). The influence of the lensing effect is mostly due to the reductions in coating materials (39.4 %, Eq. 9, Table 2). The BC absorption enhancement (E_{ab}) factor decreased by 0.003 due to reductions in emissions (Fig. 4b). We further quantified that the reduced

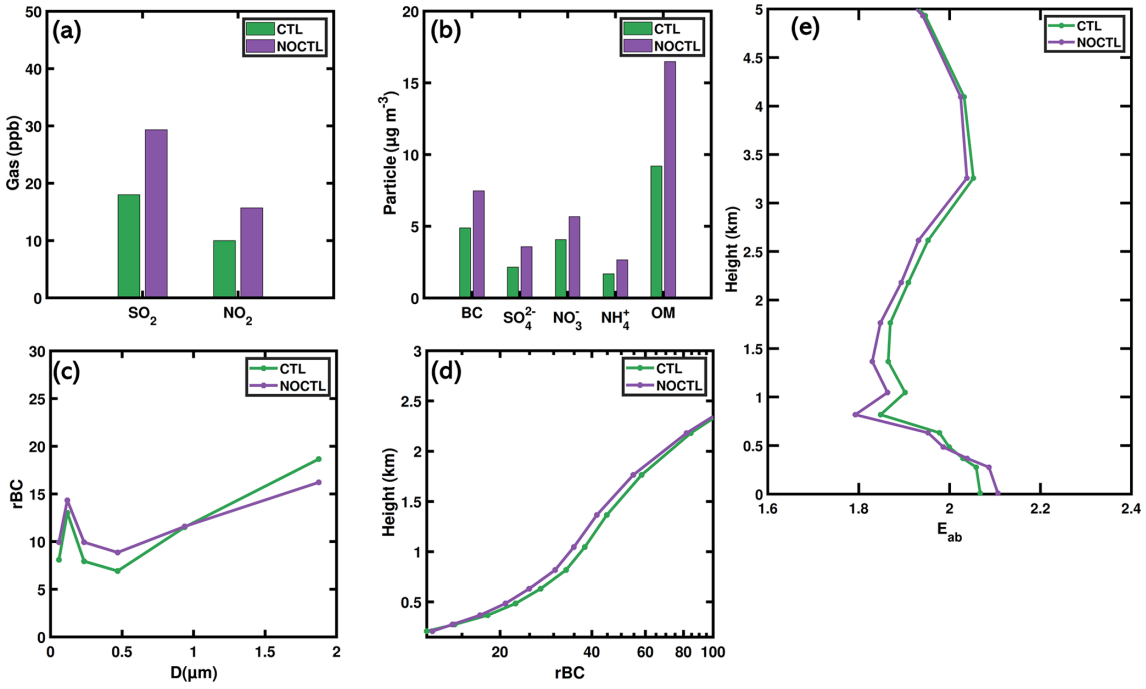

Figure 3. Mass concentrations of gaseous and condensed pollutants in the CTL and NOCTL cases **(a–b)**; the distribution of *r*BC with sizes in the CTL and NOCTL cases **(c)**; the distribution of *r*BC with height in the CTL and NOCTL cases **(d)** and the distribution of E_{ab} values with height in the CTL and NOCTL cases **(e)**.

light absorption capability (E_{ab}) resulting from emission reductions during APEC contributed 3.2 % to the total reductions in AAOD (Eq. 10, Table 2).

3.4 Influences on boundary layer process and air pollution

The vertical distribution of BC absorption plays an important role in modulating the temperature gradient and changing boundary layer meteorology (Ding et al., 2016). We conducted a series of numerical experiments to understand the influences of reshaped BC absorption due to emission reductions during APEC on boundary layer process and the formation of air pollution. Figure 4c illustrates the vertical profiles of BC absorption induced changes in the equivalent potential temperature (EPT), which is commonly used to indicate the stability of air in the atmosphere (Obremski et al., 1989). When EPT decreases with height, the atmosphere is unstable, and vertical motion and convection is likely to occur. In all experiments, BC absorption induces a positive impact on EPT in the air above ground acting to enhance the stability of the atmosphere (Fig. 4c). The maximum enhancement occurs at layers close to 1–2 km (Fig. 4c). At ∼ 2.6 km, the maximum ratio of changes with the core-shell model to those with an external mixing reach above 2.5, indicating the important effects of mixing state of BC in the upper boundary layer (Fig. 4c).

In urban Beijing, BC absorption induced mean changes of daytime planetary boundary layer height (PBLH) during the APEC week are −11.6 and −24.0 m for an external mixing and core-shell model, respectively (Fig. 4d). Under relatively clean conditions (CTL scenarios), these values change to −8.8 and −15.6 m for external mixing and the core-shell model for NOCTL emissions (Fig. 4d). Due to emission reductions, the impact of BC absorption on PBL inhibition decreases by 8.2 m on average during the APEC week (reduced emissions enhance PBLH by 8.2 m). The influence of reduced mass concentration of BC itself accounts for 35 % of the total changes, while the lensing effect of BC explains the rest (65 %, Table 2). The decreased coating due to emission reductions greatly contributes to the lensing effect of BC (47.4 %, Table 2).

The corresponding changes in daytime mean near-surface concentrations of O_3 and $PM_{2.5}$ in Beijing are displayed in Fig. 4e and f, respectively. The inhibited development of PBL due to BC absorption results in a higher abundance of $PM_{2.5}$ within the PBL (Ding et al., 2016; Gao et al., 2016b). Previously, we quantified that the cobenefits of reduced aerosol feedback could explain ∼ 11 % of the total decreases in $PM_{2.5}$ in Beijing during APEC. Here we focus on the light absorption of BC, and find that the lensing effect of BC decreases $PM_{2.5}$ concentration by 0.8 μg m^{-3} on average (Fig. 4f). On average, declines in BC mass concentration itself account for 64.3 % of the total impact of reduced light absorption of BC on $PM_{2.5}$, while 35.7 % is attributed

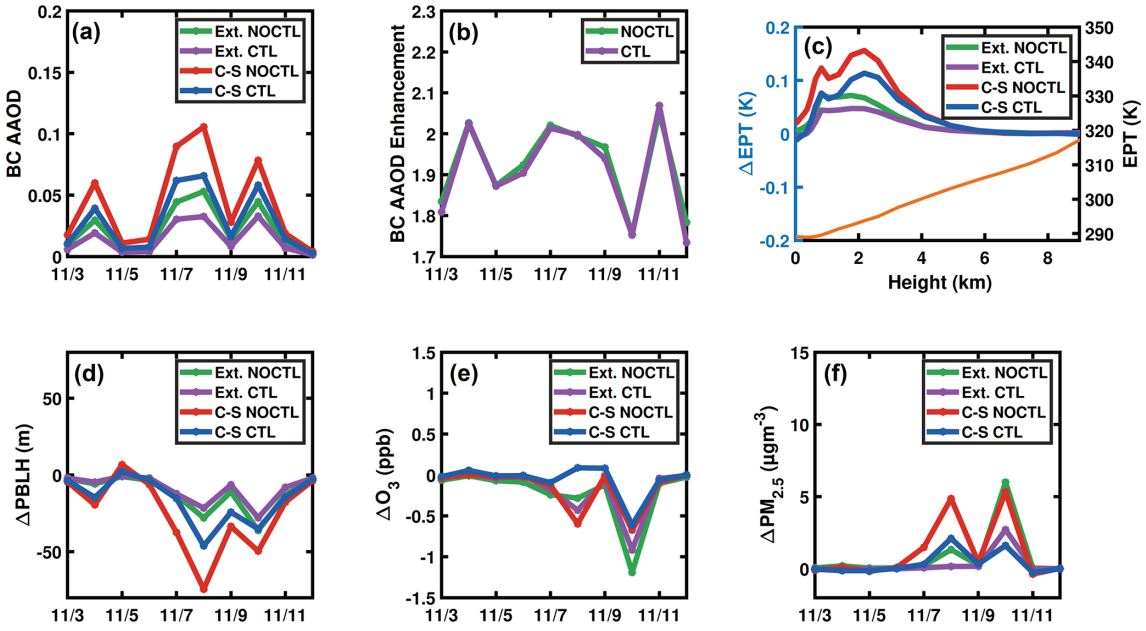

Figure 4. Daytime (10:00–17:00 local time) mean BC AAOD in Beijing inferred from different simulations **(a)** and the BC AAOD enhancement in the NOCTL and CTL scenarios **(b)**; BC absorption induced changes in EPT (orange line indicates the vertical profile of EPT) **(c)**, PBLH **(d)**, O_3 **(e)**, and $PM_{2.5}$ **(f)**.

Table 2. The division of the impact of BC absorption into the impact of BC mass itself and the BC mixing state.

Influenced variables	BC mass itself	BC lensing effect	Reduced coating	Reduced E_{ab}
AAOD	52.0 %	48.0 %	39.4 %	3.2 %
PBLH	34.9 %	65.1 %	47.4 %	–
$PM_{2.5}$	64.3 %	35.7 %	–	–
O_3	49.1 %	50.9 %	–	–

to the lensing effect of BC. However, inhibited PBL development does not necessarily lead to enhanced levels of near-surface O_3, as the formation of O_3 is also affected by changes in aerosols and photolysis reactions above the ground (Chen et al., 2021; Lu et al., 2019). As displayed in Fig. 4e, near-surface O_3 concentrations in urban Beijing decrease in response to BC absorption.

The spatial distribution of $\Delta_{\text{emission-Ext}}$ and $\Delta_{\text{emission-CS}}$ in Fig. 5 reveals that external mixing and core-shell models estimate similar patterns of changes in AAOD, PBLH, near-surface O_3, and near-surface $PM_{2.5}$. However, the responses of these variables are larger in the core-shell model due to the lensing effects of coating materials. Reduced emissions of BC and its coating materials during APEC led to declined AAOD, less stabilized PBLH, decreased near-surface $PM_{2.5}$ concentrations, and enhanced near-surface O_3 concentrations in the North China Plain (Fig. 5). It was noted that $PM_{2.5}$ concentrations was enhanced in northwest China, particularly when we used the C-S model. This is related to absorption-modulated natural emissions of windblown dust.

Figure 6a, b illustrates the cross sections in the northeast direction of changes in BC absorption coefficient due to emission reductions, as Beijing and polluted cities in South Hebei are covered. Pronounced declines are concentrated below 2 km, and the core-shell model estimates stronger reductions due to lensing effects (Fig. 6c). Emission control measures also reshaped the light absorption enhancement factor of BC, as indicated in Fig. 6f. Within the lower boundary layer, E_{ab} values were reduced with emission reductions during APEC. Light absorption of BC stabilizes boundary layer to accumulate $PM_{2.5}$, yet this effect is inhibited at lower emission levels during APEC. These relationships are reflected in Fig. 6g and h with negative changes in $PM_{2.5}$ near the ground.

The responses of O_3 to reduced light absorption of BC during APEC are in the opposite direction (Gao et al., 2018c), compared to those for $PM_{2.5}$. Strong absorption of BC tends to enhance photolysis above the aerosol layer, but to reduce photolysis near the ground. Figure 7d, g illustrate the changes in O_3 1D and NO_2 photolysis rates with emission reductions inferred from an external mixing assumption. With emission

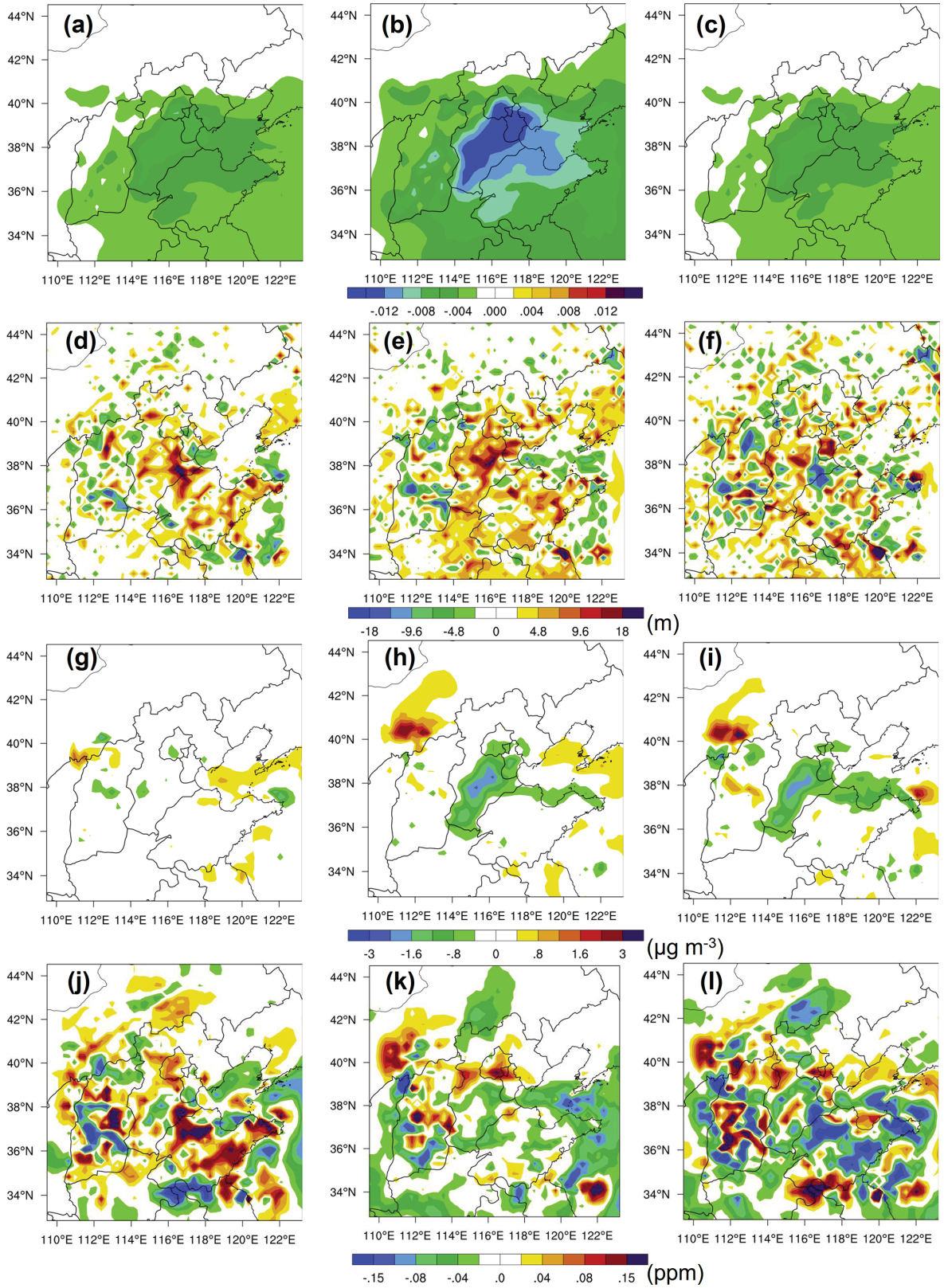

Figure 5. Spatial distribution of daytime (10:00–17:00 local time) mean BC AAOD (first row), and mean BC absorption induced changes after emission reductions (CTL minus NOCTL) in PBLH (second row), $PM_{2.5}$ (third row), and O_3 (fourth row); first, second, and third columns represent $\Delta_{\text{emission-Ext}}$, $\Delta_{\text{emission-CS}}$, and Δ_{aging}.

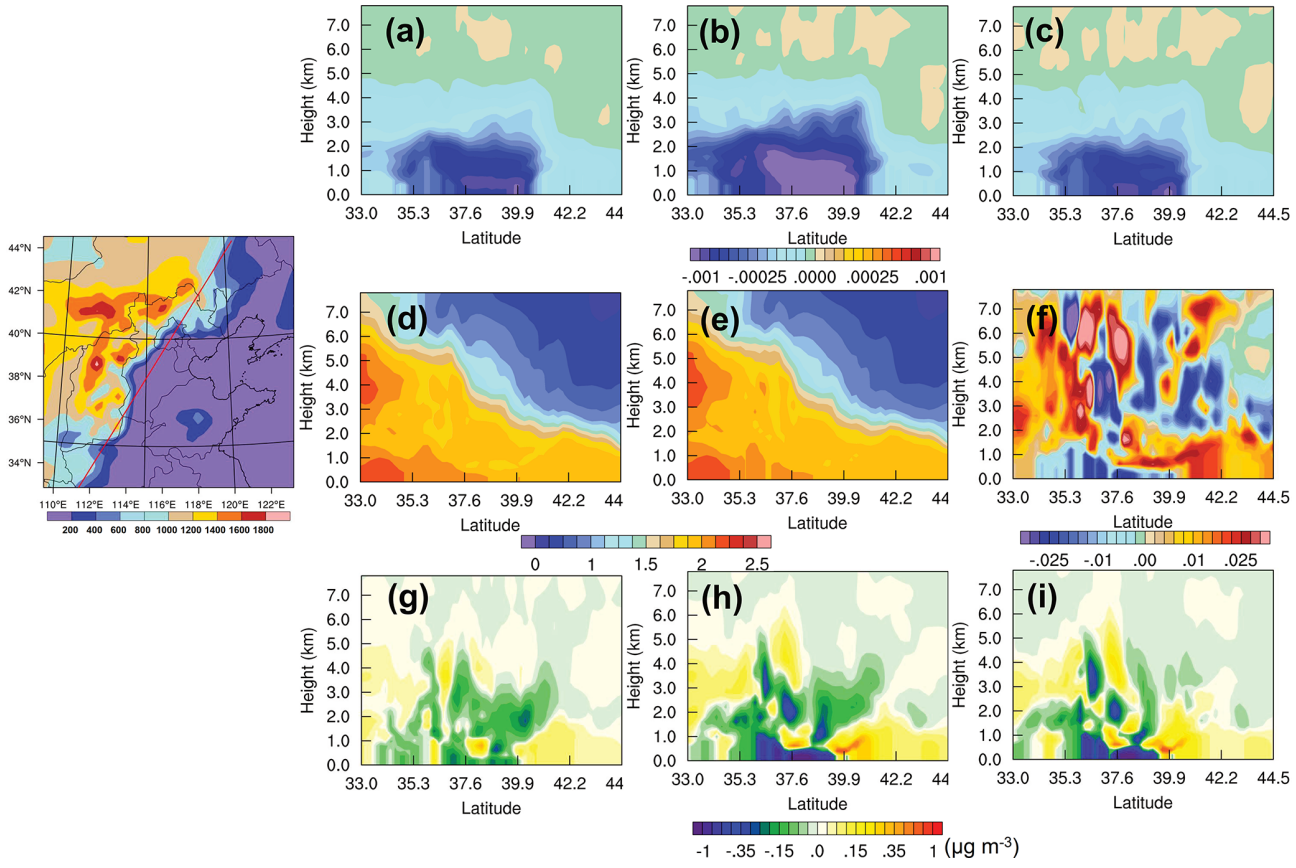

Figure 6. Cross sections of daytime (10:00–17:00 local time) mean changes in BC absorption coefficient (first row, CTL minus NOCTL), E_{ab} (second row), BC absorption induced changes after emission reductions (CTL minus NOCTL) in $PM_{2.5}$ (third row); first, second, and third columns represent $\Delta_{emission\text{-}Ext}$, $\Delta_{emission\text{-}CS}$, and Δ_{aging}.

control implemented, photolysis rates near the ground are enhanced due to lower light absorption of BC, while the photolysis rates above the aerosol layer are reduced. Similar patterns but with larger values are found using the core-shell model (Fig. 7e, h). The responses of O_3 are generally in line with the responses of O_3 1D and NO_2 photolysis rates (Fig. 7a, b).

4 Summary and discussions

In this study, we used the online coupled WRF-Chem model to understand how emission control measures during the APEC event would affect the mixing state and light absorption of BC, and the implications for BC-PBL interactions. Multiple observations, including surface observations of meteorological variables, $PM_{2.5}$, $PM_{2.5}$ chemical composition, and AAOD were used to evaluate model performance. A series of numerical experiments were conducted to address three questions: (1) how did emission reductions affect the aging processes and light absorption of BC during APEC; (2) what were the relative contributions of the reduced mass concentrations of BC, aging processes of BC, and reshaped mixing state of BC, to the changes in light absorption of BC during APEC; and (3) how did these processes affect BC-PBL interactions and the formation of air pollution?

We found that both the mass concentration of BC and the BC coating materials declined during the APEC week, which reduced the light absorption and light absorption enhancement (E_{ab}) of BC. Below 500 m in the troposphere, emission reductions during APEC lowered the absorption enhancement factor E_{ab} from 2.11 to 2.06. The column absorption enhancement was also reduced. The reduced AAOD during APEC is caused by both the declines in mass concentration of BC itself (52.0 %) and the lensing effect of BC (48.0 %). The reductions in coating materials (39.4 %) contributed the most to the influence of the lensing effect, and the reduced light absorption capability (E_{ab}) contributed 3.2 % to the total reductions in AAOD. Our estimate of the contribution of reduced light absorption capability (E_{ab}) exhibits lower values than Zhang et al. (2016), which could be caused by the uncertainties in the assumption of the mixing state of BC in the core-shell model.

The diminished light absorption of BC during APEC promotes the development of PBL, as indicated in the changes

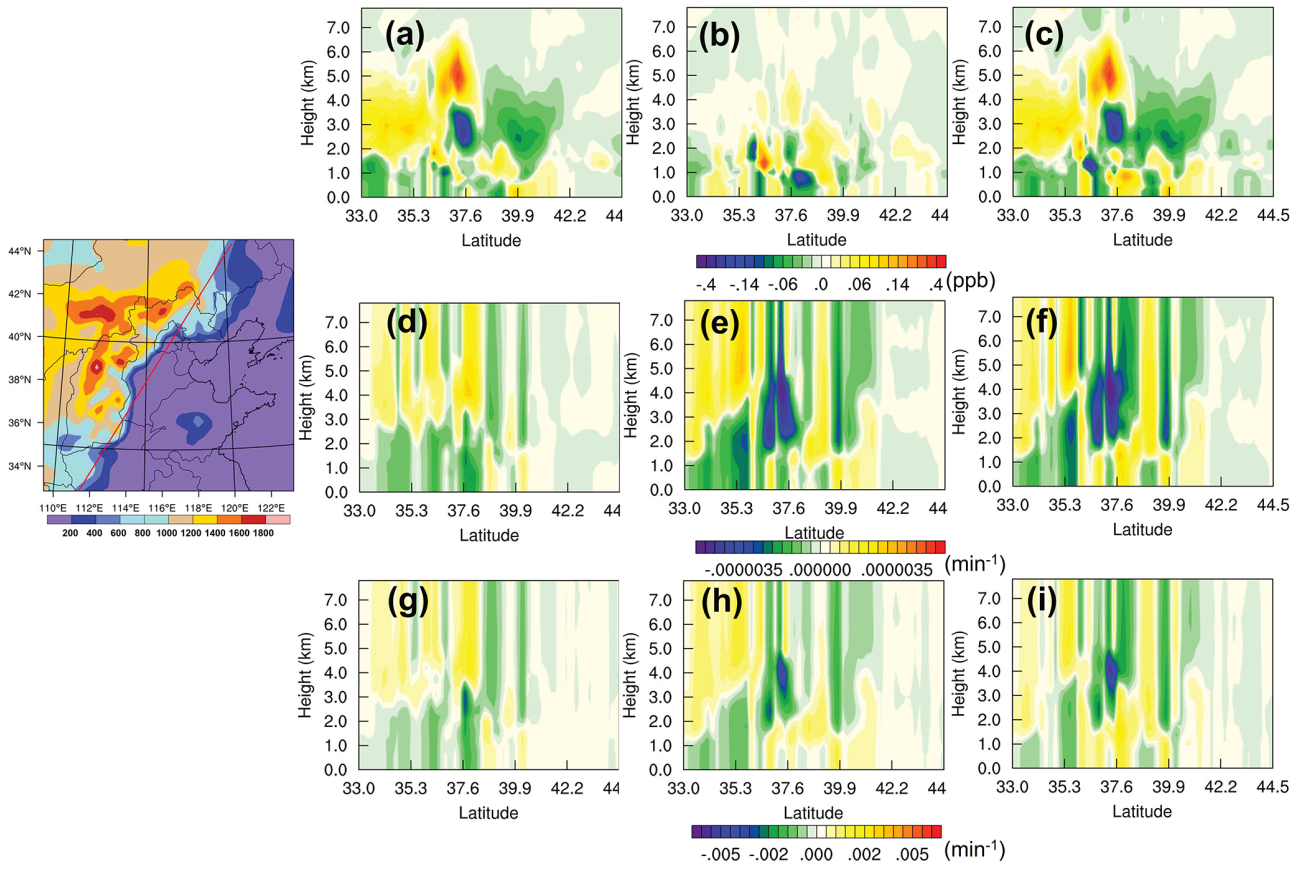

Figure 7. Cross sections of daytime (10:00–17:00 local time) mean changes in BC absorption induced changes after emission reductions (CTL minus NOCTL) in O_3 (first row), O_3 1D photolysis rate (second row), and NO_2 photolysis rate (third row); first, second and third columns represent $\Delta_{\text{emission-Ext}}$, $\Delta_{\text{emission-CS}}$, and Δ_{aging}.

in vertical profiles of EPT. Different responses of $PM_{2.5}$ and O_3 were found to the changes in the light absorption of BC. The responses of $PM_{2.5}$ follow the enhanced PBLH in decreasing, while O_3 concentrations increase near the ground. The enhanced levels of O_3 were mainly caused by the influences of BC absorption on photolysis rates. As displayed in the conceptual scheme plot in Fig. 8, reduced emissions of BC and its coating materials during APEC led to declined AAOD, less stabilized PBLH, decreased near-surface $PM_{2.5}$ concentrations, and enhanced near-surface O_3 concentrations in the North China Plain.

This study with perturbations of emissions during APEC offers important implications for the potential effects of China's Clean Air Act. As discussed in our previous investigation (Gao et al., 2017), emission control measures have the cobenefits of reducing aerosol feedback to accelerate the cleaning of air, which accounts for $\sim 11\,\%$ of the decreased $PM_{2.5}$ concentrations during APEC. In this study, we further clarified that the ongoing measures to control SO_2, NO_x, etc. would be effective in reducing the absorption capability of BC to inhibit the feedback of BC on the boundary layer. Our results also show that near-ground O_3 responds differently

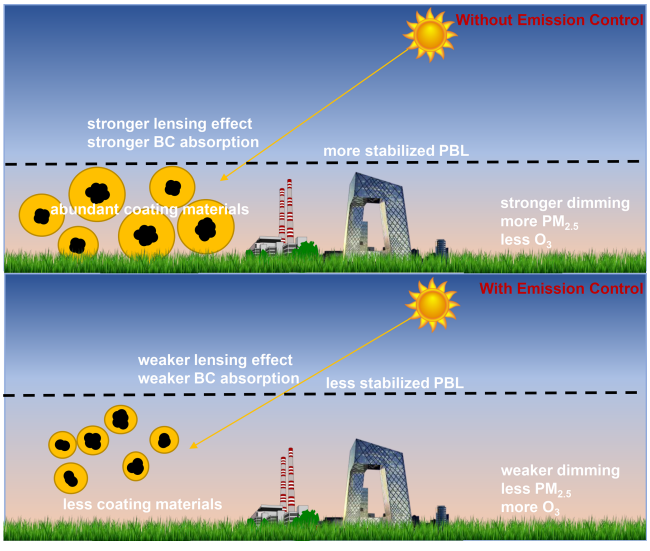

Figure 8. Conceptual scheme of the effects of emission control during APEC on the light absorption capability of BC, PBL, and air quality.

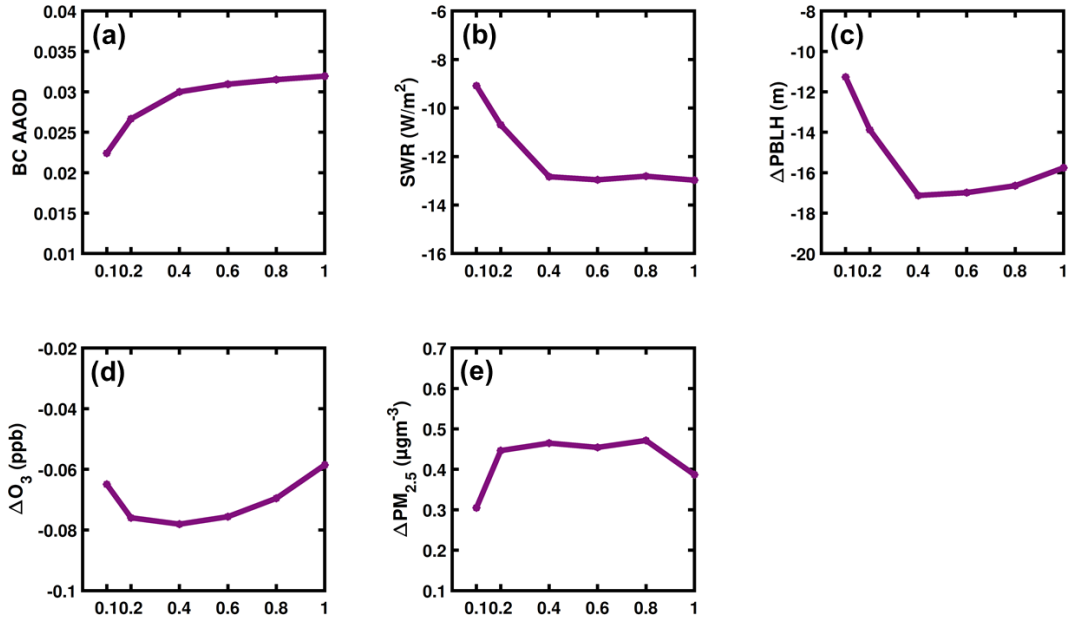

Figure 9. Daytime (10:00–17:00 local time) mean BC AAOD in Beijing **(a)** BC absorption induced changes in shortwave radiation **(b)**, PBLH **(c)**, O_3 **(d)**, and $PM_{2.5}$ **(e)** as a function of the fraction of non-BC particles mixed with BC.

from the changes in $PM_{2.5}$, which might be a side effect of current emission control strategies. Ma et al. (2021) reported that aerosol radiative effect could explain 23 % of the total change in surface summertime O_3 in China. How to control emissions to offset this side effect of current emission control measures on O_3 should be an area of further focus. In addition to the influences on air quality and weather, a sudden reduction in aerosol emissions may potentially affect climate (Ren et al., 2020; Yang et al., 2020), which warrants further investigation.

Although careful validation was conducted in this study, uncertainties still remain in the current study. We concluded that the core-shell model captures the variation of AAOD better than an external mixing assumption. However, the core-shell model is an ideal scenario that assumes all non-BC materials are internally mixed and coated on BC (Miyakawa et al., 2014). Zhang et al. (2016) observed that BC particles are heavily coated and are in a near-spherical shape in the North China Plain. The usage of the core-shell model seems to be reasonable in this study, whereas the assumption that all non-BC materials are coated on BC might not be true in real atmospheric conditions. The observed ratio of coatings to PM_1 was $\sim$ 25 %–70 % in summer in Beijing (Xu et al., 2019), and the observed ratio of coatings to $PM_{2.5}$ was $\sim$ 10 %–40 % in winter in Beijing (Wang et al., 2019). We conducted additional simulations assuming 10 %, 20 %, 40 %, 60 %, and 80 % mixing fractions of coating aerosols, and explored how these assumptions would affect estimated BC AAOD, and its feedback on radiation, the boundary layer, and air pollutants. As suggested in Fig. 9, modeled BC AAOD increases gradually when the mixing fraction rises from 0.1 to 0.4, but it keeps relatively stable when the mixing fraction is between 0.4 and 1. The responses of near-surface shortwave radiation and PBLH are in line with it, exhibiting relatively constant reductions when the mixing fraction is higher than 0.4 (Fig. 9). However, no significant relationships are found for BC absorption induced changes in O_3 (< 10 % difference between fractions of 0.1 and 1) and $PM_{2.5}$ (< 22 % difference between fractions of 0.1 and 1) in Beijing. These results suggest that the findings demonstrated in this study might not be largely affected by the assumptions in mixing fractions of coating particles. Additionally, the simulated feedback of BC absorption on boundary layer processes are not well constrained. We used multiple coupled models to examine how these processes are represented, and we calculated the ensemble mean to optimize understanding (Gao et al., 2018a, 2020a). In the future, further efforts are needed to constrain the uncertainties of these processes in the model.

Data availability. The measurements and model simulations data can be accessed by contacting the corresponding authors.

Supplement. The supplement related to this article is available online at: https://doi.org/10.5194/acp-21-11405-2021-supplement.

Author contributions. MG and JH designed the study. MG performed model simulations and analyzed the data with help from YY, HL, BZ, YZ, XL, CW, QZ and GRC. QZ provided the emis-

sion inventory. YW and ZL provided measurements. MG and JH wrote the paper with inputs from all the other authors.

Competing interests. The authors declare that they have no conflict of interest.

Disclaimer. Publisher's note: Copernicus Publications remains neutral with regard to jurisdictional claims in published maps and institutional affiliations.

Financial support. This work was supported by the Open fund by Jiangsu Key Laboratory of Atmospheric Environment Monitoring and Pollution Control (grant no. KHK1902), the National Key Research and Development Program of China (grant no. 2016YFA0602003), the National Natural Science Foundation of China (no. 42005084 and no. 92044302), the Ministry of Science and Technology of the People's Republic of China (Grant no. 2017YFC0210000), the Natural Science Foundation of Guangdong Province (no. 2019A1515011633), and special fund of the State Key Joint Laboratory of Environment Simulation and Pollution Control (grant no. 19K03ESPCT).

Review statement. This paper was edited by James Allan and reviewed by two anonymous referees.

References

Ackerman, T. P. and Toon, O. B.: Absorption of visible radiation in atmosphere containing mixtures of absorbing and non-absorbing particles, Appl. Optics, 20, 3661–3662, 1981.

Andreae, M. O. and Gelencsér, A.: Black carbon or brown carbon? The nature of light-absorbing carbonaceous aerosols, Atmos. Chem. Phys., 6, 3131–3148, https://doi.org/10.5194/acp-6-3131-2006, 2006.

Barnard, J. C., Fast, J. D., Paredes-Miranda, G., Arnott, W. P., and Laskin, A.: Technical Note: Evaluation of the WRF-Chem "Aerosol Chemical to Aerosol Optical Properties" Module using data from the MILAGRO campaign, Atmos. Chem. Phys., 10, 7325–7340, https://doi.org/10.5194/acp-10-7325-2010, 2010.

Bond, T. C., Streets, D. G., Yarber, K. F., Nelson, S. M., Woo, J., and Klimont, Z.: A technology-based global inventory of black and organic carbon emissions from combustion, J. Geophys. Res.-Atmos., 109, D14203, https://doi.org/10.1029/2003JD003697, 2004.

Bond, T. C., Habib, G., and Bergstrom, R. W.: Limitations in the enhancement of visible light absorption due to mixing state, J. Geophys. Res., 111, D20211, https://doi.org/10.1029/2006JD007315, 2006.

Bond, T. C., Doherty, S. J., Fahey, D. W., Forster, P. M., Berntsen, T., Deangelo, B. J., Flanner, M. G., Ghan, S., Kärcher, B., Koch, D., Kinne, S., Kondo, Y., and Quinn, P. K.: Bounding the role of black carbon in the climate system: A scientific assessment, J. Geophys. Res.-Atmos., 118, 5380–5552, https://doi.org/10.1002/jgrd.50171, 2013.

Cappa, C. D., Onasch, T. B., Massoli, P., Worsnop, D. R., Bates, T. S., Cross, E. S., Davidovits, P., Hakala, J., Hayden, K. L., Jobson, B. T., Kolesar, K. R., Lack, D. A., Lerner, B. M., Li, S. M., Mellon, D., Nuaaman, I., Olfert, J. S., Petaja, T., Quinn, P. K., Song, C., Subramanian, R., Williams, E. J., and Zaveri, R. A.: Radiative Absorption Enhancements Due to the Mixing State of Atmospheric Black Carbon, Science, 337, 1078–1081, 2012.

Chen, D., Liao, H., Yang, Y., Chen, L., and Wang, H.: Simulated aging processes of black carbon and its impact during a severe winter haze event in the Beijing-Tianjin-Hebei region, Sci. Tot. Env., 755, 142712, https://doi.org/10.1016/j.scitotenv.2020.142712, 2021.

Chen, Y., Beig, G., Archer-Nicholls, S., Drysdale, W., Acton, J., Lowe, D., Nelson, B. S., Lee, J. D., Ran, L., Wang, Y., Wu, Z., Sahu, S. K., Sokhi, R. S., Singh, V., Gadi, R., Hewitt, C. N., Nemitz, E., Archibald, A., McFiggins, G., and Wild, O.: Avoiding high ozone pollution in Delhi, India, Faraday Discuss., 226, 502–514, https://doi.org/10.1039/D0FD00079E, 2021.

Cheng, Y., Zheng, G., Wei, C., Mu, Q., Zheng, B., Wang, Z., Gao, M., Zhang, Q., He, K., Carmichael, G., Pöschl, U., and Su, H.: Reactive nitrogen chemistry in aerosol water as a source of sulfate during haze events in China, Sci. Adv., 2, e1601530, https://doi.org/10.1126/sciadv.1601530, 2016.

Ching, J., Riemer, N., and West, M.: Impacts of black carbon particles mixing state on cloud microphysical properties: sensitivity to environmental conditions, J. Geophys. Res.-Atmos., 121, 5990–6013, https://doi.org/10.1002/2016JD024851, 2016.

Curci, G., Alyuz, U., Barò, R., Bianconi, R., Bieser, J., Christensen, J. H., Colette, A., Farrow, A., Francis, X., Jiménez-guerrero, P., Im, U., and Liu, P.: Modelling black carbon absorption of solar radiation: combining external and internal mixing assumptions, Atmos. Chem. Phys., 19, 181–204, https://doi.org/10.5194/acp-19-181-2019, 2019.

Curtis, J. H., Riemer, N., and West, M.: A single-column particle-resolved model for simulating the vertical distribution of aerosol mixing state: WRF-PartMC-MOSAIC-SCM v1.0, Geosci. Model Dev., 10, 4057–4079, https://doi.org/10.5194/gmd-10-4057-2017, 2017.

Ding, A. J., Huang, X., Nie, W., Sun, J. N., Kerminen, V., Petäjä, T., Su, H., Cheng, Y. F., Yang, X., Wang, M. H., Chi, X. G., Wang, J. P., Virkkula, A., Guo, W. D., Yuan, J., Wang, S. Y., Zhang, R. J., Wu, Y. F., Song, Y., Zhu, T., Zilitinkevich, S., Kulmala, M., and Fu, C. B.: Enhanced haze pollution by black carbon in megacities in China, Geophys. Res. Lett., 43, 2873–2879, https://doi.org/10.1002/2016GL067745, 2016.

Dubovik, O. and King, M. D.: A flexible inversion algorithm for retrieval of aerosol optical properties from Sun and sky radiance measurements A flexible inversion algorithm for retrieval of aerosol optical properties from Sun and sky radiance measurements, J. Geophys. Res.-Atmos., 105 20673–20696, https://doi.org/10.1029/2000JD900282, 2000.

Emmons, L. K., Walters1, S., Hess1, P. G., Lamarque, J.-F., Pfister1, G. G., Fillmore1, D., Granier, C., Guenther, A., Kinnison, D., Laepple1, T., Orlando, J., Tie, X., Tyndall, G., Wiedinmyer, C., Baughcum, S. L., and Kloster, S.: Description and evaluation of the Model for Ozone and Related chemical Trac-

ers, version 4 (MOZART-4), Geosci. Model Dev., 3, 43–67, https://doi.org/10.5194/gmd-3-43-2010, 2010.

Flanner, M. G., Zender, C. S., Randerson, J. T., and Rasch, P. J.: Present-day climate forcing and response from black carbon in snow Present-day climate forcing and response from black carbon in snow, J. Geophys. Res.-Atmos., 112, D11202, https://doi.org/10.1029/2006JD008003, 2007.

Fuller, K. A., Malm, W. C., and Kreidenweis, S. M.: Effects of mixing on extinction by carbonaceous particles Effects of mixing on extinction by carbonaceous particles, J. Geophys. Res.-Atmos., 104, 15941–15954, https://doi.org/10.1029/1998JD100069, 1999.

Gao, M., Carmichael, G. R., Wang, Y., Ji, D., Liu, Z., and Wang, Z.: Improving simulations of sulfate aerosols during winter haze over Northern China: the impacts of heterogeneous oxidation by NO_2, Front. Environ. Sci. Technol., 10, 1–11, https://doi.org/10.1007/s11783-016-0878-2, 2016a.

Gao, M., Carmichael, G. R., Wang, Y., Saide, P. E., Yu, M., Xin, J., Liu, Z., and Wang, Z.: Modeling study of the 2010 regional haze event in the North China Plain, Atmos. Chem. Phys., 16, 1673–1691, https://doi.org/10.5194/acp-16-1673-2016, 2016b.

Gao, M., Liu, Z., Wang, Y., Lu, X., Ji, D., and Wang, L.: Distinguishing the roles of meteorology, emission control measures, regional transport, and co-benefits of reduced aerosol feedback in "APEC" Blue, Atmos. Environ., 167, 476–486, https://doi.org/10.1016/j.atmosenv.2017.08.054, 2017.

Gao, M., Han, Z., Liu, Z., Li, M., Xin, J., Tao, Z., and Li, J.: Air Quality and Climate Change, Topic 3 of the Model Inter-Comparison Study for Asia Phase III (MICS-Asia III), Part I: overview and model evaluation, Atmos. Chem. Phys., 18, 4859–4884, https://doi.org/10.5194/acp-18-4859-2018, 2018a.

Gao, M., Ji, D., Liang, F., and Liu, Y.: Attribution of aerosol direct radiative forcing in China and India to emitting sectors, Atmos. Environ., 190, 35–42, https://doi.org/10.1016/j.atmosenv.2018.07.011, 2018b.

Gao, J., Zhu, B., Xiao, H., Kang, H., Pan, C., Wang, D., and Wang, H.: Effects of black carbon and boundary layer interaction on surface ozone in Nanjing, China, Atmos. Chem. Phys., 18, 7081–7094, https://doi.org/10.5194/acp-18-7081-2018, 2018c.

Gao, M., Han, Z., Tao, Z., Li, J., Kang, J.-E., Huang, K., Dong, X., Zhuang, B., Li, S., Ge, B., Wu, Q., Lee, H.-J., Kim, C.-H., Fu, J. S., Wang, T., Chin, M., Li, M., Woo, J.-H., Zhang, Q., Cheng, Y., Wang, Z., and Carmichael, G. R.: Air quality and climate change, Topic 3 of the Model Inter-Comparison Study for Asia Phase III (MICS-Asia III) – Part 2: aerosol radiative effects and aerosol feedback, Atmos. Chem. Phys., 20, 1147–1161, https://doi.org/10.5194/acp-20-1147-2020, 2020a.

Gao, M., Liu, Z., Zheng, B., Ji, D., Sherman, P., Song, S., Xin, J., Liu, C., Wang, Y., Zhang, Q., Xing, J., Jiang, J., Wang, Z., and Carmichael, G. R.: China's emission control strategies have suppressed unfavorable influences of climate on wintertime $PM_{2.5}$ concentrations in Beijing since 2002, Atmos. Chem. Phys., 20, 1497–1505, https://doi.org/10.5194/acp-20-1497-2020, 2020b.

Gao, M., Gao, J., Zhu, B., Kumar, R., Lu, X., Song, S., Zhang, Y., and Jia, B.: Ozone pollution over China and India: seasonality and sources, Atmos. Chem. Phys., 20, 4399–4414, https://doi.org/10.5194/acp-20-4399-2020, 2020c.

Giglio, L., Randerson, J. T., and Van Der Werf, G. R.: Analysis of daily, monthly, and annual burned area using the fourth-generation global fire emissions database (GFED4), J. Geophys. Res.-Biogeo., 118, 317–328, https://doi.org/10.1002/jgrg.20042, 2013.

Grell, G. A., Peckham, S. E., Schmitz, R., Mckeen, S. A., Frost, G., Skamarock, W. C., and Eder, B.: Fully coupled "online" chemistry within the WRF model, Atmos. Environ., 39, 6957–6975, https://doi.org/10.1016/j.atmosenv.2005.04.027, 2005.

Grieshop, A. P., Reynolds, C. C. O., Kandlikar, M., and Dowlatabadi, H.: A black-carbon mitigation wedge, Nat. Publ. Gr., 2, 533–534, https://doi.org/10.1038/ngeo595, 2009.

Guenther, A., Karl, T., Harley, P., Wiedinmyer, C., Palmer, P. I., and Geron, C.: Estimates of global terrestrial isoprene emissions using MEGAN (Model of Emissions of Gases and Aerosols from Nature), Atmos. Chem. Phys., 6, 3181–3210, https://doi.org/10.5194/acp-6-3181-2006, 2006.

Holben, B. N., Slutsker, T. I. E. I., Tar, D., Buis, J. P., Setxerj, I. I. A., Reagan, A., J, Y., Nakajima, T., Lavenu, F., Vemte, E., Jankowiak, I., and Smirnozjt, A.: AERONET-A Federated Instrument Network and Data Archive for Aerosol Characterization, Remote Sens. Environ., 66, 1–16, 1998.

Hong, S.-Y.: A new stable boundary-layer mixing scheme and its impact on the simulated East Asia summer monsoon, Q. J. Roy. Meteorol. Soc., 136, 1481–1496, 2010.

IPCC: Climate Change 2014: Synthesis Report, Contribution of Working Groups I, II and III to the Fifth Assessment Report of the Intergovernmental Panel on Climate Change, edited by: Core Writing Team, Pachauri, R. K., and Meyer, L. A.,151 pp., IPCC, Geneva, Switzerland, 2014.

Jacobson, M. Z.: Strong radiative heating due to the mixing state of black carbon in atmospheric aerosols, Nature, 409, 695–697, https://doi.org/10.1038/35055518, 2001.

Ji, D., He, J., Sun, Y., and Gao, M.: Two-year continuous measurements of carbonaceous aerosols in urban Beijing, China: Temporal variations, characteristics and source analyses, Chemosphere, 200, 191–200, https://doi.org/10.1016/j.chemosphere.2018.02.067, 2018.

Ji, D., Gao, W., Maenhaut, W., He, J., Wang, Z., Li, J., Du, W., Wang, L., Sun, Y., Xin, J., Hu, B., and Wang, Y.: Impact of air pollution control measures and regional transport on carbonaceous aerosols in fine particulate matter in urban Beijing, China: insights gained from long-term measurement, Atmos. Chem. Phys., 19, 8569–8590, https://doi.org/10.5194/acp-19-8569-2019, 2019a.

Ji, D., Gao, M., Maenhaut, W., He, J., Wu, C., Cheng, L., Gao, W., Sun, Y., Sun, J., Xin, J., Wang, L., and Wang, Y.: The carbonaceous aerosol levels still remain a challenge in the Beijing-Tianjin-Hebei region of China: Insights from continuous high temporal resolution measurements in multiple cities, Environ. Int., 126, 171–183, https://doi.org/10.1016/j.envint.2019.02.034, 2019b.

Li, K., Liao, H., Mao, Y., and Ridley, D. A.: Source sector and region contributions to concentration and direct radiative forcing of black carbon in China, Atmos. Environ., 124, 351–366, https://doi.org/10.1016/j.atmosenv.2015.06.014, 2016.

Li, M., Zhang, Q., Kurokawa, J., Woo, J., He, K., Lu, Z., and Ohara, T.: MIX: a mosaic Asian anthropogenic emission inventory under the international collaboration framework of the MICS-Asia and HTAP, Atmos. Chem. Phys., 17, 935–963, https://doi.org/10.5194/acp-17-935-2017, 2017.

Liang, F., Gao, M., Xiao, Q., Carmichael, G. R., Pan, X., and Liu, Y.: Evaluation of a data fusion approach to estimate daily $PM_{2.5}$ levels in North China, Environ. Res., 158, 54–60, 2017.

Liu, D., Whitehead, J., Alfarra, M. R., Reyes-villegas, E., Spracklen, D. V, Reddington, C. L., Kong, S., Williams, P. I., Ting, Y., Haslett, S., Taylor, J. W., Flynn, M. J., Morgan, W. T., Mcfiggans, G., Coe, H., and Allan, J. D.: Black-carbon absorption enhancement in the atmosphere determined by particle mixing state, Nat. Geosci., 10, 184–188, https://doi.org/10.1038/NGEO2901, 2017.

Liu, Z., Hu, B., Zhang, J., Xin, J., Wu, F., Gao, W., Wang, M., and Wang, Y.: Characterization of fine particles during the 2014 Asia-Pacific economic cooperation summit: Number concentration, size distribution and sources, Tellus B, 69, 1303228, https://doi.org/10.1080/16000889.2017.1303228, 2017.

Lu, X., Zhang, L., Zhao, Y., Jacob, D. J., Hu, Y., Hu, L., Gao, M., Liu, X., Petropavlovskikh, I., McClure-Begley, A., and Querel, R.: Surface and tropospheric ozone trends in the Southern Hemisphere since 1990: possible linkages to poleward expansion of the Hadley circulation, Sci. Bull., 64, 400–409, https://doi.org/10.1016/j.scib.2018.12.021, 2019.

Ma, X., Huang, J., Zhao, T., Liu, C., Zhao, K., Xing, J., and Xiao, W.: Rapid increase in summer surface ozone over the North China Plain during 2013–2019: a side effect of particulate matter reduction control?, Atmos. Chem. Phys., 21, 1–16, https://doi.org/10.5194/acp-21-1-2021, 2021.

Matsui, H., Koike, M., Kondo, Y., Moteki, N., Fast, J. D., and Zaveri, R. A.: Development and validation of a black carbon mixing state resolved three-dimensional model: Aging processes and radiative impact, J. Geophys. Res.-Atmos., 118, 2304–2326, https://doi.org/10.1029/2012JD018446, 2013.

Matsui, H.: Black carbon simulations using a size-and mixing-state-resolved three-dimensional model: 1. Radiative effects and their uncertainties, J. Geophys. Res.-Atmos., 121, 1793–1807, https://doi.org/10.1002/2015JD023998, 2016.

Menon, S., Hansen, J., Nazarenko, L., and Luo, Y.: Climate Effects of Black Carbon Aerosols in China and India, Science, 297, 2250–2253, https://doi.org/10.1126/science.1075159, 2002.

Miyakawa, T., Takeda, N., Koizumi, K., Tabaru, M., Ozawa, Y., Hirayama, N., and Takegawa, N.: A new lase induced incandescence – mass spectrometric analyzer (LII-MS) for online measurement of aerosol composition classified by black carbon mixing state, Aerosol Sci. Tech., 48, 853–863, 2014.

Obremski, J., Samson, J., Dutkiewicz, V., and Husain, L.: On the use of surface equivalent potential temperature in isolating the influence of local as opposed to transported sources on aerosol concentrations, J. Geophys. Res.-Atmos., 94, 11117–11127, https://doi.org/10.1029/JD094iD08p11117, 1989.

Onasch, C. D. C. T. B., Massoli, P., Worsnop, D. R., Bates, T. S., Cross, E. S., Davidovits, P., Hakala, J., Hayden, K. L., Jobson, B. T., Katheryn R., Kolesar, D. A. L., Lerner, B. M., Li, S.-M., Mellon, D., Nuaaman, I., Olfert, J. S., Petäjä, T., Quinn, P. K., Song, C., Subramanian, R., Williams, E. J., and Zaveri, R. A.: Radiative Absorption Enhancements Due to the Mixing State of Atmospheric Black Carbon, Science, 337, 1078–1081, https://doi.org/10.1126/science.1223447, 2012.

Pan, Y., Tian, S., Liu, D., Fang, Y., Zhu, X., Gao, M., Wentworth, G.R., Michalski, G., Huang, X., and Wang, Y.: Source Apportionment of Aerosol Ammonium in an Ammonia-Rich Atmosphere: An Isotopic Study of Summer Clean and Hazy Days in Urban Beijing, J. Geophys. Res.-Atmos., 123, 5681–5689, 2018.

Peng, J., Hu, M., Guo, S., Du, Z., Zheng, J., Shang, D., Levy, M., and Zeng, L.: Markedly enhanced absorption and direct radiative forcing of black carbon under polluted urban environments, P. Natl. Acad. Sci. USA, 113, 4266–4271, https://doi.org/10.1073/pnas.1602310113, 2016.

Qin, W., Zhang, Y., Chen, J., Yu, Q., Cheng, S., Li, W., Liu, X., and Tian, H.: Variation, sources and historical trend of black carbon in Beijing, China based on ground observation and MERRA-2 reanalysis data, Environ. Pollut., 245, 853–863, https://doi.org/10.1016/j.envpol.2018.11.063, 2019.

Ramanathan, V. and Carmichael, G. R.: Global and regional climate changes due to black carbon, Nat. Geosci., 1, 221–227, https://doi.org/10.1038/ngeo156, 2008.

Ren, L., Yang, Y., Wang, H., Zhang, R., Wang, P., and Liao, H.: Source attribution of Arctic black carbon and sulfate aerosols and associated Arctic surface warming during 1980–2018, Atmos. Chem. Phys., 20, 9067–9085, https://doi.org/10.5194/acp-20-9067-2020, 2020.

Schuster, G. L., Dubovik, O., and Holben, B. N.: Angstrom exponent and bimodal aerosol size distributions, J. Geophys. Res., 111, D07207, https://doi.org/10.1029/2005JD006328, 2006.

Shrivastava, M., Easter, R. C., Northwest, P., Zaveri, R. A., Northwest, P., Saide, P. E., and Angeles, L.: Modeling organic aerosols in a megacity: comparison of simple and complex representations of the volatility basis set approach, Atmos. Chem. Phys., 11, 6639–6662, https://doi.org/10.5194/acp-11-6639-2011, 2011.

Tian, J., Riemer, N., West, M., Pfaffenberger, L., Schlager, H., and Petzold, A.: Modeling the evolution of aerosol particles in a ship plume using PartMC-MOSAIC, Atmos. Chem. Phys., 14, 5327–5347, https://doi.org/10.5194/acp-14-5327-2014, 2014.

Toon, O. B. and Ackerman, T. P.: Algorithms for the calculation of scattering by stratified spheres, Appl. Opt., 20, 3657–3660, 1981.

Wang, J., Liu, D., Ge, X., Wu, Y., Shen, F., Chen, M., Zhao, J., Xie, C., Wang, Q., Xu, W., Zhang, J., Hu, J., Allan, J., Joshi, R., Fu, P., Coe, H., and Sun, Y.: Characterization of black carbon-containing fine particles in Beijing during wintertime, Atmos. Chem. Phys., 19, 447–458, https://doi.org/10.5194/acp-19-447-2019, 2019.

Xu, W., Xie, C., Karnezi, E., Zhang, Q., Wang, J., Pandis, S. N., Ge, X., Zhang, J., An, J., Wang, Q., Zhao, J., Du, W., Qiu, Y., Zhou, W., He, Y., Li, Y., Li, J., Fu, P., Wang, Z., Worsnop, D. R., and Sun, Y.: Summertime aerosol volatility measurements in Beijing, China, Atmos. Chem. Phys., 19, 10205–10216, https://doi.org/10.5194/acp-19-10205-2019, 2019.

Yamineva, Y. and Liu, Z.: Cleaning the air, protecting the climate: Policy, legal and institutional nexus to reduce black carbon emissions in China, Environ. Sci. Policy, 95, 1–10, https://doi.org/10.1016/j.envsci.2019.01.016, 2019.

Yang, Y., Wang, H., Smith, S. J., Ma, P.-L., and Rasch, P. J.: Source attribution of black carbon and its direct radiative forcing in China, Atmos. Chem. Phys., 17, 4319–4336, https://doi.org/10.5194/acp-17-4319-2017, 2017.

Yang, Y., Smith, S. J., Wang, H., Mills, C. M., and Rasch, P. J.: Variability, timescales, and nonlinearity in climate responses to black carbon emissions, Atmos. Chem. Phys., 19, 2405–2420, https://doi.org/10.5194/acp-19-2405-2019, 2019.

Yang, Y., Ren, L., Li, H., Wang, H., Wang, P., Chen, L., Yue, X., and Hong, L.: Fast climate responses to aerosol emission reductions during the COVID-19 pandemic, Geophys. Res. Lett., 47, e2020GL089788, https://doi.org/10.1029/2020GL089788, 2020.

Zaveri, R. A. and Peters, L. K.: A new lumped structure photochemical mechanism for long-scale applications, J. Geophys. Res.-Atmos., 104, 30387–30415, https://doi.org/10.1029/1999JD900876, 1999.

Zaveri, R. A., Easter, R. C., Fast, J. D., and Peters, L. K.: Model for Simulating Aerosol Interactions and Chemistry (MOSAIC), J. Geophys. Res., 113, D13204, https://doi.org/10.1029/2007JD008782, 2008.

Zhang, Q., Zheng, Y., Tong, D., Shao, M., Wang, S., Zhang, Y., and Xu, X.: Drivers of improved $PM_{2.5}$ air quality in China from 2013 to 2017, P. Natl. Acad. Sci. USA, 116, 24463–24469, https://doi.org/10.1073/pnas.1907956116, 2019.

Zhang, Y., Zhang, Q., Cheng, Y., Su, H., Kecorius, S., Wang, Z., Wu, Z., Hu, M., Zhu, T., Wiedensohler, A., and He, K.: Measuring the morphology and density of internally mixed black carbon with SP2 and VTDMA: new insight into the absorption enhancement of black carbon in the atmosphere, Atmos. Meas. Tech., 9, 1833–1843, https://doi.org/10.5194/amt-9-1833-2016, 2016.

Zhang, Y., Li, X., Li, M., Zheng, Y., Geng, G., Hong, C., Li, H., Tong, D., Zhang, X., Cheng, Y., Su, H., He, K., and Zhang, Q.: Reduction in black carbon light absorption due to multi-pollutant emission control during APEC China 2014, Atmos. Chem. Phys., 18, 10275–10287, https://doi.org/10.5194/acp-18-10275-2018, 2018.

Zhang, Y., Li, M., Cheng, Y., Geng, G., Hong, C., Li, H., Li, X., and Tong, D.: Modeling the aging process of black carbon during atmospheric transport using a new approach: a case study in Beijing, Atmos. Chem. Phys., 19, 9663–9680, https://doi.org/10.5194/acp-19-9663-2019, 2019.

Zheng, B., Tong, D., Li, M., Liu, F., Hong, C., Geng, G., Li, H., Li, X., and Peng, L.: Trends in China's anthropogenic emissions since 2010 as the consequence of clean air actions, Atmos. Chem. Phys., 18, 14095–14111, https://doi.org/10.5194/acp-18-14095-2018, 2018.

Zhou, W., Gao, M., He, Y., Wang, Q., Xie, C., Xu, W., Zhao, J., Du, W., Qiu, Y., Lei, L., and Fu, P.: Response of aerosol chemistry to clean air action in Beijing, China: Insights from two-year ACSM measurements and model simulations, Environ. Pollut., 255, 113345, https://doi.org/10.1016/j.envpol.2019.113345, 2019.